Evolution of the Crystalline Texture of High-Density Polyethylene during Uniaxial Compression

Z. Bartczak,† R. E. Cohen,*,‡ and A. S. Argon*,§

Departments of Chemical and Mechanical Engineering, Massachusetts Institute of Technology, Cambridge, Massachusetts 02139-4307

Received January 13, 1992; Revised Manuscript Received May 12, 1992

ABSTRACT: The formation of an axially symmetrical texture in high-density polyethylene (HDPE) was studied through uniaxial compression at room temperature. The orientation of crystallographic axes was probed at various stages of the deformation process, up to an equivalent strain of 1.86, by means of WAXS pole figures. Additionally the lamellar orientation was studied using small-angle X-ray scattering (SAXS) and transmission electron microscopy (TEM). The results of these structural and morphological studies demonstrated that the major deformation mechanism involved in plastic deformation of the crystalline parts of the sample was the (100)[001] chain slip. Other mechanisms that were detected as active in the crystalline phase were (100)[010] transverse slip, and, to a lesser extent, twinning and martensitic transformations. Plastic deformation of the crystalline phase was accompanied by deformation of the amorphous phase, mostly by shear of the interlamellar layers (interlamellar sliding). Such shear was found to be partially reversible, especially at lower strains. In contrast to other deformation modes, the deformation of HDPE by uniaxial compression does not induce fragmentation of the lamellar superstructure, at least in the strain range studied.

1. Introduction

Over the past 30 years many aspects of deformation behavior of semicrystalline polymers, including studies of morphological changes during deformation, have been extensively studied (see refs 1-3). Most of the theoretical and experimental studies of deformation considered linear polyethylene. The deformation process of polyethylene was investigated in a wide variety of initial morphologies (single crystals, oriented material with various textures, spherulitic thin films, and bulk specimens) as well as in a variety of deformation geometries (uniaxial and biaxial drawing, solid-state extrusion, rolling, plane strain, and uniaxial compression). It is now well established that in much of the irreversible plastic deformation of polyethylene, up to reasonably high strains, the deformation mechanisms involved are mostly crystallographic in nature, quite similar to those found in the plastic deformation of metal single crystals and many other low-molecular weight crystalline materials. Among these mechanisms, the crystallographic slip modes in the chain direction are the most important. In addition to the deformation mechanisms operating in the crystals, some deformation mechansims acting in the amorphous layers between lamellae are also involved in the early phase of the deformation process. The simultaneous activity of several deformation mechanisms allows the initial structure to be transformed in a continuous manner to the final oriented state. All of the above-mentioned mechanisms have been reviewed in the past.[1-3] In some deformation conditions, especially cold drawing, the large-strain deformation seems to involve a discontinuous transformation of the structure from its initial unoriented to final oriented state. However, the nature of that process is still not fully clarified in the literature. A commonly accepted model of this transformation, referred to as "micronecking", was proposed by Peterlin.[4] According to this model the lamellae during the drawing undergo an abrupt fragmentation and unfolding into much smaller crystalline blocks from which the dense-packed microfibrils are subsequently drawn out. Partial melting and recrystallization have also been invoked in the process of reconstitution of the crystal structure. On the other hand, some experimental results of small- and wide-angle X-ray diffraction taken at various stages of deformation[5-7] may suggest that the transformation from the initially isotropic to the eventual fibrous structure is still continuous, although complex. In our recent study of the morphological alterations during plane strain compression we have demonstrated that while the overall deformation history from the initial, unoriented spherulitic type to the final fully aligned form may involve some internal inhomogeneities, this process is much more continuous than realized in the past.[8]

The goal of the present study was to investigate in detail the changes of the texture and morphology of bulk, spherulitic polyethylene step by step during large-strain plastic deformation in uniaxial compression. Most of the previously reported studies of the structural changes caused by deformation were performed in a tensile mode, guided by obvious technological stimuli to explain processes associated with orientation by drawing. However, from the fundamental point of view the deformation by compression is of equal importance. Moreover, uniaxial compression has the great advantage that the deformation is nearly a homogeneous process and occurs without any significant deformation instabilities such as those observed in tensile drawing when necks are formed. Therefore, in uniaxial compression it is possible to monitor the evolution of the texture and morphology of the material continuously over the whole range of the applied strain. In spite of these advantages we were able to locate only one report describing the evolution of structure during the uniaxial compression of initially spherulitic polyethylene.[9] In the present study the uniaxial compression mode was chosen because of its geometrical simplicity and lack of external constraints, which allows also parallel computer simulation of the deformation process with relative ease and accuracy. Details of this simulation study and comparison of its results with the morphological observations reported here are presented in a separate paper.[10]

2. Experimental Section

2.1. Materials and Sample Preparation. The material used in this study was high-density polyethylene (HDPE), Petroth-

† Permanent address: Centre of Molecular and Macromolecular Studies, Polish Academy of Sciences, 90-362 Lodz, Poland.
‡ Department of Chemical Engineering.
§ Department of Mechanical Engineering.

0024-9297/92/2225-4692$03.00/0

Table I
Deformation Parameters of Specimens Studied

specimen no.	applied strain, ϵ	final strain, ϵ_p[a]	final compression λ_p ratio
1	0.09	0.02	1.02
2	0.16	0.05	1.05
3	0.28	0.10	1.11
4	0.49	0.20	1.22
5	0.60	0.35	1.42
6	1.00	0.73	2.08
7	1.08	0.82	2.27
8	1.28	1.03	2.80
9	1.50	1.29	3.63
10	1.82	1.61	5.00
11	2.05	1.86	6.42

[a] After a 24-h period of recovery.

ene LS 606-00, supplied by USI Division, Quantum, Cincinnati, OH. Its molecular weight is M_w = 55 000 with a polydispersity ratio of M_w/M_n = 4.8, melt flow index 9–11 g/10 min (ASTM D-1238), and density 0.941–0.980 g/cm^3.

The polymer pellets were compression molded at 180 °C and 100 atm of pressure to form a plate of 20-mm thickness. The mold was cooled at a moderate rate, so that the spherulitic superstructure inside the plate could fully develop (the spherulite size in the core of the plate was in the range of 5 μm, as estimated by light microscopy; the overall crystallinity exceeds 70%). From the molded plates the outer skin layers (at least 5 mm from each side) were removed by machining. As revealed by X-ray measurements, the core of the obtained plates had no traces of any crystallographic orientation anisotropy, which might be a result of compression molding. From that completely unoriented material the cylindrical specimens were machined out for the deformation studies. The thickness of the machined disks was varied in the range of 1.5–11 mm depending on the intended strain, in order to obtain all the deformed samples with a similar thickness of ca. 1.5 mm. The corresponding diameters of the disk specimens varied in the range of 15–27 mm. The diameter of the specimens was selected to be as large as possible in order to eliminate the influence of any possible inhomogeneity or instability of the deformation (which could possibly occur on the specimen edge) on the results of structural investigations. The X-ray diffraction patterns were taken from the central part of the specimens, covering a diameter of a few millimeters for any orientation of the specimen viewed by the incident X-ray beam; the usual diameter of the whole deformed specimen was ca. 27 mm.

The initially unoriented specimens were compressed uniaxially at room temperature with a constant strain rate of 1×10^{-3} s^{-1} using an Instron testing machine (Model 1350). The constant strain rate was controlled in the course of the whole deformation by a computer connected on-line to the Instron machine. In order to reduce the friction between the compression steel plates and the compressed specimen, pairs of thin Teflon foils (each 20 μm thick) were placed on both compression surfaces of the specimens. The specimens, deformed to a certain strain, were held under load for 15 min before slow load release. The specimens were deformed in a single compression step up to a true strain of 1.6 (compression ratio 6). Because of the load limitation of the Instron machine the higher strains had to be achieved in two compression steps, between which the specimen diameter was reduced by remachining. The thickness of the specimens was measured prior to deformation, immediately after unloading, and also in some predetermined time intervals within the next 24 h. On the basis of the thickness measurements, the permanent compression ratio and hence permanent true strain, as well as strain recovery in the unloaded state, were calculated. The data for the specimens used in the study are listed in Table I. No structural studies were performed until the strain recovery had ceased (at least 24 h after unloading).

2.2. X-ray Measurement. The overall orientations of crystallographic planes of the original and deformed samples were determined by means of an automated computer-controlled Rigaku wide-angle X-ray scattering (WAXS) system consisting of a pole figure device associated with a wide-angle goniometer coupled to a rotating-anode X-ray generator operating at 50 kV and 60 mA (Cu Kα radiation, filtered electronically and by a Ni filter). The complete pole figures were obtained for projection of Euler angles of sample orientation with respect to the incident beam, α from 0° to 90° in 2° intervals and β from 0° to 360° in 10° steps. The construction of complete pole figures required the connection of the X-ray data collected in both transmission and reflection modes; the connection angle, α_c, was 40°. The necessary corrections for background scattering and sample absorption were calculated and pole figures were constructed by DMAXB software (Rigaku). Pole figures for the following crystal planes were constructed: (110), (200), (020), and (011).

The changes in the lamellar orientation in the compressed samples were studied by means of small-angle X-ray scattering measurements (SAXS). The SAXS measurements were performed using another system consisting of a Siemens two-dimensional position-sensitive detector and a second Rigaku rotating-anode fine-point X-ray generator emitting Cu Kα radiation, operating at 40 kV and 30 mA. The primary beam was collimated by a two-mirror collimating system consisting of Ni mirrors. The specimen to detector distance of the SAXS system was 2.3 m. The scattered X-ray path between the specimen and detector was enclosed by a tube filled with He gas to minimize background scattering. The time of data collection was usually 10 min, although shorter exposure times were also used.

Changes of lamellar orientation were also studied by SAXS on smaller specimens (about 4 mm in diameter) deformed directly in the SAXS camera using small compression clamps, so that the specimen remained under load during the measurement; these specimens were also examined after load release. Using the same experimental setup, but with a short sample–detector distance (8 cm), the two-dimensional WAXS patterns were recorded for specimens under load and after load release. These WAXS specimens were compressed to strains very close to those imposed on the specimens examined by SAXS.

2.3. Microscopy. The morphologies of the original and compressed specimens were examined by means of a polarizing light microscope (Nikon Optiphot-Pol) in 1-μm-thick sections microtomed perpendicular to the specimen radius.

For the purpose of electron microscopy studies, all the initial and deformed specimens were first stained and fixed in chlorosulfonic acid at 60 °C for 20 h.[12] After staining, the ultrathin sections were cut out from the samples with the same orientation as in the sections for light microscopy. The sectioning of stained samples was performed at room temperature using a LKB Ultramicrotome V equipped with freshly prepared glass knives. The sections were examined using a Philips 300 transmission electron microscope operating at 100 kV.

2.4. Density Measurements. Densities of the samples were determined by means of a 1-m-long gradient column filled with a mixture of ethyl alcohol and water. The temperature of the column was maintained at 23 °C.

3. Results

3.1. Macroscopic Behavior. Figure 1 presents a typical true stress–true strain curve obtained for HDPE uniaxially compressed at room temperature. After the usual initial elastic response there is a region of intense plastic deformation and flow, followed by strain hardening which starts at true axial strains in the range of 0.8–0.9. The stress at the yield point may be estimated as 27.5 MPa. The arrows on this plot indicate the points in the deformation history at which detailed structural studies were carried out. The accompanying numbers in boxes indicate the permanent strain after strain recovery for 24 h.

The deformed samples showed large amounts of strain recovery after releasing the load. The instantaneous elastic recovery was followed by another, longer, and time-dependent recovery process, which was quite intense in the first few minutes after unloading, then slowed down, and was almost complete within 2 h. The recovery ceased completely within the next few hours. This process is

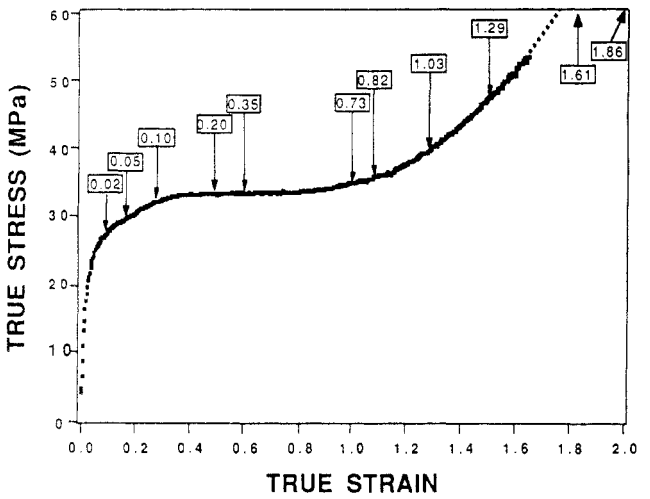

Figure 1. Typical true stress–true strain curve obtained for the HDPE deformed in uniaxial compression at room temperature. The arrows indicate the strains at which detailed structural studies were made; the numbers indicate the permanent strain after strain recovery for 24 h.

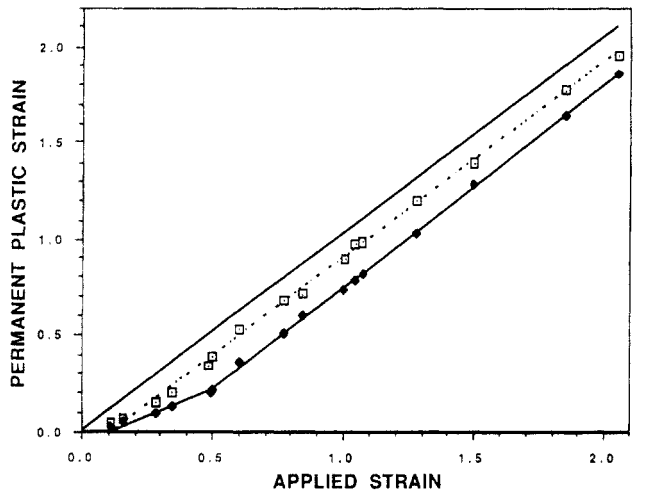

Figure 2. Dependence of the transient strain ϵ_t (measured immediately after unloading) and permanent plastic strain ϵ_p (measured 24 h after unloading and strain recovery) on the applied strain. The dashed line shows the initial elastic recovery and the solid line the total strain after "free" recovery of the specimens.

illustrated in Figure 2, where the transient plastic strain shown by open squares (as measured just after elastic recovery) and the final, permanent plastic strain, shown as solid diamonds, is plotted as a function of the strain imposed on the sample under load. It is seen that the elastic part of the recovery is constant and independent of the imposed strain (consistent with little or no strain hardening until a true strain of about 1.0) whereas the time-dependent component is a function of the strain. It increases initially from 0 to about 0.2 with increasing applied strain up to a true strain of 0.5 (where the corresponding permanent strain is around 0.2). The amount of recoverable strain then remains nearly constant until a level of strain around 1.0 is reached, and then it begins to decrease slowly with further applied strain. It may be seen that these changes follow approximately the changes in the character of the stress–strain curve—both stress and recovery initially increase, the region of constant recovery corresponds to the flat part of stress–strain curve of little or no hardening, and recovery decreases after the onset of the strong strain hardening. Clearly, this time-dependent strain recovery is associated not only with the release of residual stresses due to plastic inhomogeneities but also with the reversal of some inelastic deformation.

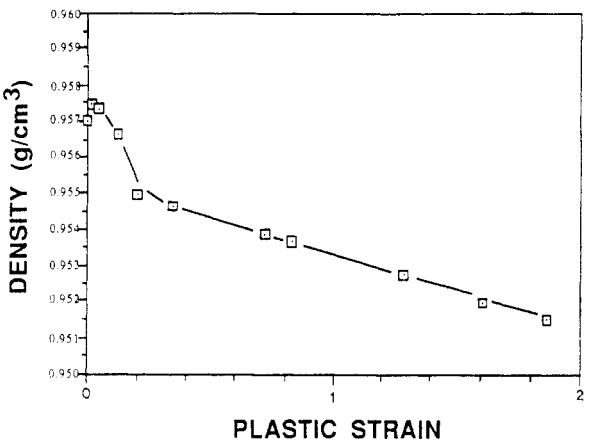

Figure 3. Changes of the density as a function of permanent plastic strain.

The density change of the samples as a function of permanent strain ϵ_p is presented in Figure 3. After a slight increase during the initial stages of deformation, the density decreases monotonically with a further strain increase. The slope of the curve is higher for smaller strains. This change of slope occurs at a plastic strain around $\epsilon_p = 0.2$. The observed density changes are probably the result of two competing processes: (i) a decrease of the overall crystallinity due to an increasing number of the crystal defects generated during deformation and even partial destruction of some crystals and (ii) an increase of the density of the amorphous phase caused by permanent orientation.[12] This second effect probably becomes more pronounced at true permanent strains above 0.2. Note that this break occurs at the point where strain recovery saturates, as can be seen by comparison with Figure 2.

3.2. Changes of Morphology. Figure 4 shows light optical micrographs of the sections cut from unoriented and deformed specimens. The sections were cut perpendicular to the radius of the samples, i.e., along the loading direction, LD. In the unoriented specimen and those deformed to small strains ($\epsilon_p < 0.35$; Figure 4a,b) the spherulitic structure can be observed and shows little change due to straining. At somewhat higher strains ($\epsilon_p = 0.73$; Figure 4c) the spherulites are more difficult to recognize, although they are still intact. At a permanent strain $\epsilon_p = 0.82$ (Figure 4d), a new feature of the deformation process appears: the deformation tends to localize in the form of densely packed fine shear bands tilted with respect to the loading direction. With increasing strain these bands widen and tilt gradually away from LD (see Figure 4e,f). The deformation, although partially localized in the shear bands, remains macroscopically homogeneous because of the fine character of these bands and their dense, space-filling nature.

Figure 5 presents a series of electron micrographs of the ultrathin sections cut from the strained samples; in all cases the cut was parallel to LD. The staining agent was chlorosulfonic acid which preferentially stained amorphous layers and did not affect the crystalline phase.[11] Because of the relation between the lamellar thickness (100–200 Å) and the thickness of the section (ca. 700 Å), only those lamellae oriented edge-on in the section can be clearly seen in the microscope. In undeformed specimens there is no preferred orientation of the lamellae, so only a certain fraction of them can be seen on the micrograph, those that are oriented edge-on in the section. Visible lamellae are oriented at every angle with respect to LD (see Figure 5a). The number of recognizable lamellae slightly increases

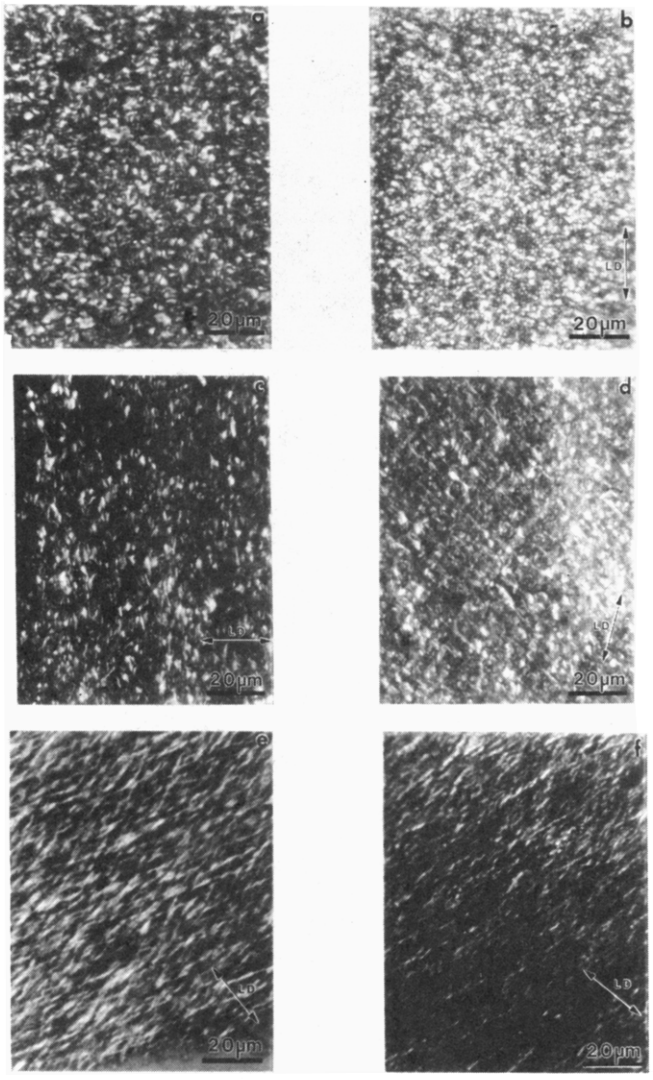

Figure 4. Light optical micrographs (under crossed polarizers) of sections cut perpendicular to the radius vector from the samples deformed to various permanent strains: (a) undeformed, (b) 0.10, (c) 0.73, (d) 0.82, (e) 1.29, (f) 1.86. The loading direction is indicated by the arrows.

with increasing strain (see Figure 5b–d) which suggests their rotation away from the loading direction. However, for true permanent strains less than 0.73 it is still rather difficult to find the direction of the preferred lamellar orientation. At a strain of $\epsilon_p = 0.73$ a preferred orientation becomes better defined as being more or less perpendicular to LD, which confirms the previous suggestion about lamellar rotation. At a strain of $\epsilon_p = 0.82$ the lamellae which were still oriented along LD undergo multiple and cooperative kinking which dramatically changes their orientation. In this way the lamellae with normals, *n* oriented perpendicular to LD are completely eliminated from the structure. As a result of the kinking process, deformation bands visible in light micrographs start to develop. The remaining lamellae improve their orientation at that time, rotating further away from LD (i.e., their normals are rotating toward LD). These features can be clearly seen in Figure 5e. Another observation which can be made on the basis of Figure 5d,e is that the lamellae that are rotating away from LD are thinner than those observed in the unoriented specimen.

At higher strains ($\epsilon_p = 1.29$ and 1.61) the above-mentioned mechanisms are still active, giving rise to the improvement of the overall orientation of the lamellae with their normals along LD. In Figure 5f,g the well-developed intense shear bands are readily recognizable as wide and bright streaks; the brightness probably arises because inside the shear bands the amorphous phase is more highly oriented than outside, making it more difficult to stain.

Finally, at a permanent strain of 1.86 (Figure 5h) the lamellae are very well oriented, with their normals distributed fairly tightly around LD. The characteristic zigzag pattern of lamellar arrangement can be clearly seen. That pattern was formed due to lamellar rotations, with some of them shearing and kinking. It is also very easy to discern in the micrograph that the lamellae, as well as the amorphous layers separating them, are now much thinner than those in the initial, undeformed polyethylene.

3.3. Small-Angle X-ray Scattering. The lamellar morphology observed in electron microscopy was further investigated by the SAXS technique. The results of these investigations are presented in Figure 6 in which the two-dimensional SAXS patterns, recorded with the incident beam perpendicular to LD i.e., in the radial direction (RD), are shown. The scattering by the unoriented sample forms a ring with a uniform intensity along all azimuthal angles, as expected from an undeformed spherulitic specimen. As permanent strain increases up to 0.73, the SAXS pattern changes systematically to an elliptical shape, with the longer axis being along LD and two maxima of the intensity developing along this direction. The intensity at these maxima increases monotonically with increasing strain, while the intensity of scattering in the perpendicular direction (along the shorter axis of the ellipse) monotonically decreases.

A significant change of the SAXS pattern occurs at $\epsilon_p = 0.82$. At that strain the SAXS pattern is no longer elliptical but more or less abruptly assumes a rather two-point shape. Closer examination of the maxima of the scattering shows, however, that they still have broadly an elliptical shape, albeit quite narrow. Thus, the pattern is still elliptical, but the scattering in the directions other than in LD is now much less intense than for specimens with smaller strains; therefore, the ellipse is very significantly depleted in the equatorial regions of the pattern. For higher strains the ellipse narrows even further, so that the scattering in directions away from LD disappears completely, and the SAXS pattern is then practically a two-point type.

The SAXS patterns were recorded also for the samples oriented with LD parallel to the incident X-ray beam. These patterns (not shown here) always had the shape of a ring, with the intensity being uniform along all azimuthal angles. Such a shape demonstrates the symmetry of deformation at the lamellar level closely parallels the symmetry of the applied load. The diameter of the rings measured at maximum intensity was equal to the length of the shorter axis of the ellipse observed in the scattering patterns with LD perpendicular to the incident beam (Figure 6). The symmetrical SAXS ring pattern was observed for all specimens with permanent strains in the range of 0–0.73. For higher strains the scattering ring quickly faded and above $\epsilon_p = 1.03$ was not observed at all, which correlates well with the change of the shape of the scattering perpendicular to LD, where the smooth transformation from the continuous ellipse to the two-point pattern was observed to begin and develop over the same range of strain.

These SAXS results support the morphological observations presented in the previous section. With increasing strain, the lamellae rotate gradually to positions at which their normals become parallel to LD, which induces the

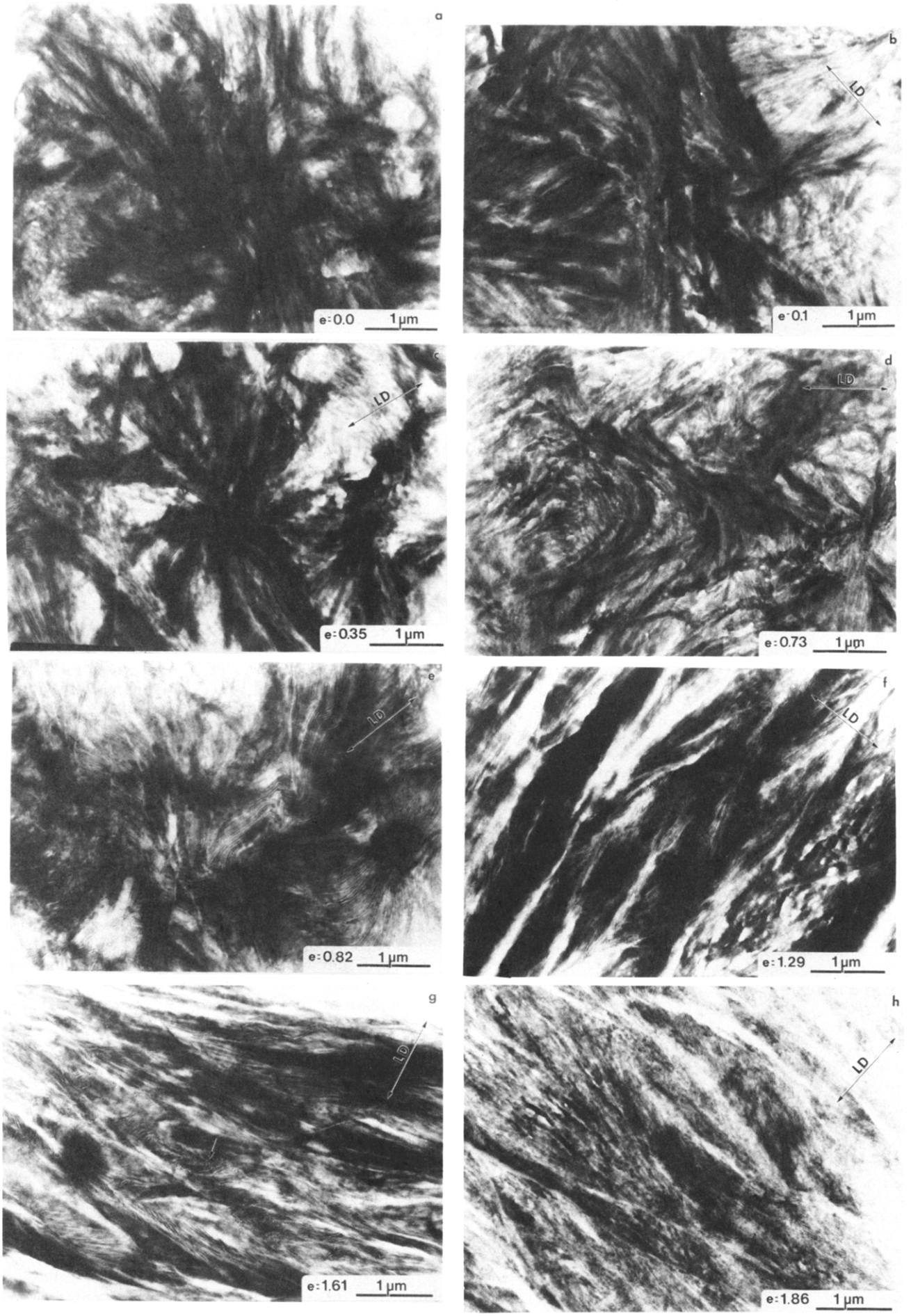

Figure 5. Transmission electron micrographs of ultrathin sections cut perpendicular to the radius vector from the samples deformed to various permanent strain and stained with chlorosulfonic acid: (a) undeformed, (b) 0.10, (c) 0.35, (d) 0.73, (e) 0.82, (f) 1.29, (g) 1.61, (h) 1.86. The loading direction is indicated by the arrows.

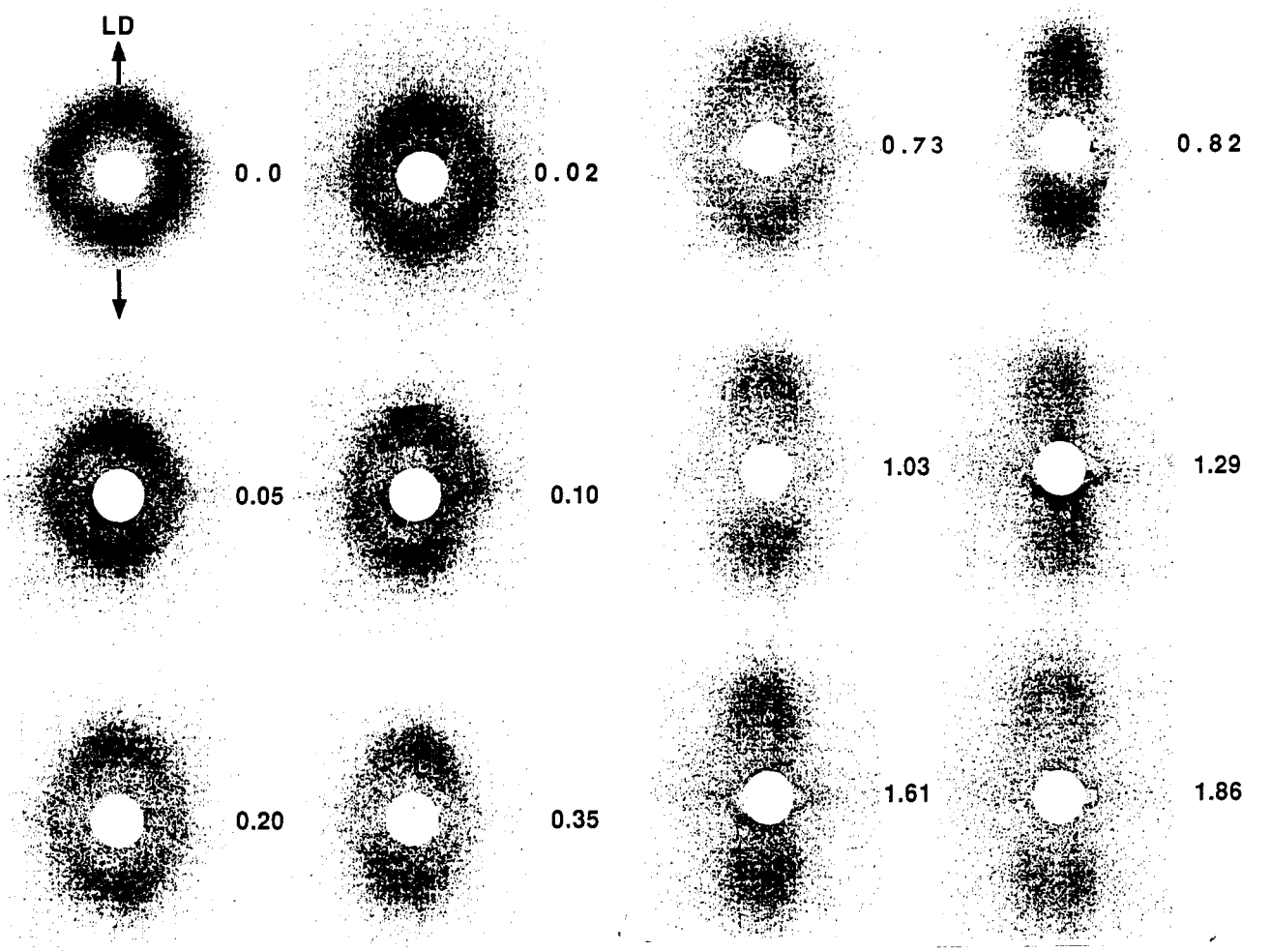

Figure 6. SAXS patterns of deformed samples recorded with the incident X-ray beam perpendicular to the loading direction. Loading direction is indicated by the arrow.

development of the scattering maxima along this direction. The number of lamellae oriented parallel to LD (normals perpendicular to LD) decreases slowly but monotonically with increasing strain for the same reason. At a permanent strain above 0.82 the lamellae oriented parallel to LD abruptly disappear. This is in excellent agreement with the morphological observations with transmission electron microscopy (TEM), which showed that in this range of strain lamellae with orientation parallel to LD undergo intense kinking, changing in this way dramatically and abruptly their orientation.

On the basis of these recorded SAXS intensities, the long periods in the direction of loading (LD) and perpendicular to it were calculated for the deformed samples. The results are shown in Figure 7, in which both values of the long period are plotted as a function of the permanent strain. The principal long period as measured along LD steadily decreases with increasing strain, which indicates thinning of the lamellae oriented with their normals close to LD and/or thinning of the amorphous layers between them which is to some extent necessary if the deformation is to satisfy compatibility and the degree of crystallinity is to be preserved. In fact the TEM observations showed the occurrence of both of these effects, although the relative change in lamellar thickness appears to be of a larger magnitude.

The shape of the dependence of the long period in the direction perpendicular to LD on strain curiously resembles the shape of the stress–strain curve; i.e., after an initial increase of the long period there is a plateau in the curve, in the strain range of 0.3–0.8, followed by another fairly

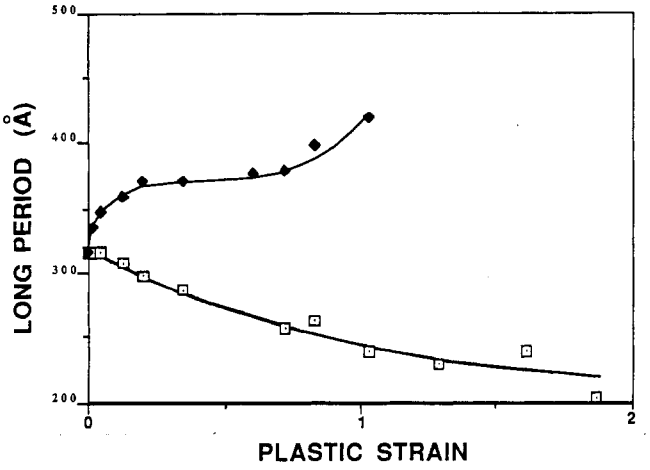

Figure 7. Dependence of the long period measured perpendicular to and parallel to the loading direction: plotted as a function of permanent strain.

sharp increase of the long period. The above changes can also be correlated with previously reported morphological observations. The initial increase of the long period may be attributed to the thickening of the amorphous material between lamellae oriented with their normals perpendicular to LD. At some point in the strain range of $\epsilon_p \approx 0.20$–0.35, the amorphous material apparently reaches its limit of extension, associated with tensioning of tie molecules which are anchored in opposite adjoining lamellae; further overall deformation does not induce further separation of these specifically oriented lamellae. The situation changes at $\epsilon_p \geq 0.82$, when widespread lamellae

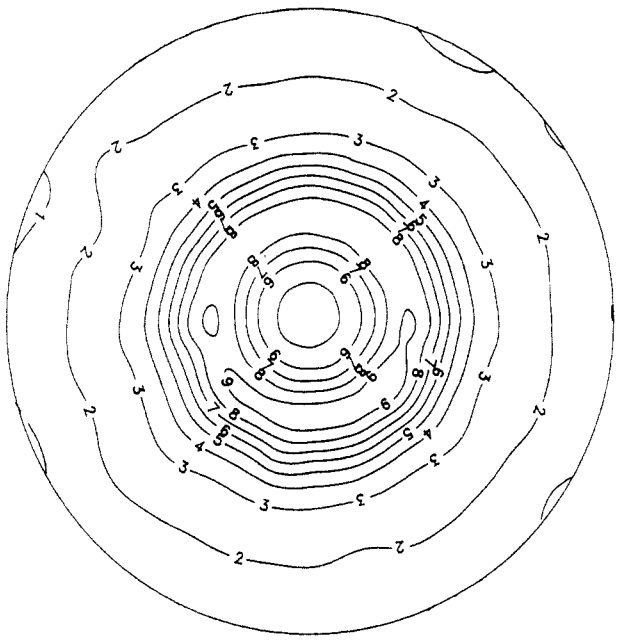

Figure 8. Pole figure of normals to (200) planes of the sample deformed to the true strain $\epsilon_p = 1.29$. The loading direction is normal to the plane of the figure.

kinking begins. During that process the lamellar crystals are likely to become extensively damaged and perhaps even pinched-off (see ref 8). This process may restructure the amorphous material and release many tie molecules, and as a consequence this may permit locally relatively large-strain, unrestricted plastic deformation to develop in the amorphous phase. As a result, more substantial thickening of the amorphous material occurs and the long period increases further. Evidence for this behavior may be seen in Figure 5g, where at the apex of the multiple kink (marked by the arrow) the thickness of the amorphous layer is recognizably much larger than in other regions of the section. It must be noted, however, that the substantially reduced SAXS intensity normal to LD indicates that only a small fraction of amorphous material is affected in this way. The disappearance of the scattering in the direction perpendicular to LD at high strain levels is also a consequence of the kinking process, where the kinking induces large reorientation of all lamellae previously oriented with their normals perpendicular to LD.

3.4. Wide-Angle X-ray Scattering. Figure 8 shows a representative pole figure of the (200) plane normals of orthorhombic polyethylene, obtained for a deformed sample at a true strain $\epsilon_p = 1.29$. A very important feature of this and all other pole figures obtained in this investigation is the axial symmetry with respect to the loading direction, which reflects the symmetry of the deformation field. This observation, together with SAXS results, supports the contention that the deformation studied was purely uniaxial, and therefore it is possible to construct, on the basis of this information, intensity vs altitude angle, α, plots to illustrate the dependence of the diffraction intensity, i.e., the pole density, on the crystallite orientations with respect to loading direction only. Such dependencies for poles of (200), (020), (110), and (011) planes were calculated from the corresponding pole figure by averaging over the azimuthal angle, β; these plots are shown in Figures 9a–d and are generally similar to those obtained recently for uniaxially compressed HDPE by Krause and Hosford.[9] From these plots the evolution of orientation of the *a* and *b* crystallographic axes can be read off directly (parts a and b of Figure 9 show the orientation of poles of (200) and (020) planes, respectively). The orientation of the *c* axis (direction of molecular alignment inside the crystal) may be deduced from either the (200) and (020) pole plots or the plots for (011) and (020) planes (Figure 9d,b; the normal to the (011) forms a 27° angle with the *c* axis in the *bc* plane). Direct visualization of the orientation of the *c* axis by measurements of the (002) reflection was not possible because of a very low signal-to-background ratio for the (002) diffraction peak, even for the highest sample orientations; this suggests a rather broad distribution of the *c* axis orientation compared to polyethylene deformed in other deformation modes.[9,13]

A detailed discussion of the deformation-induced evolution of the orientation of the orthorhombic PE crystals will be presented in section 4 below. Here we note only that from the very beginning of the plastic deformation process the *a* axes of crystallites tend to orient themselves around LD, whereas the *b* and *c* axes tend to orient approximately perpendicular to LD, i.e., close to the direction of radial flow. These tendencies persist up to the largest strain studied. The final and all intermediate textures show axial symmetry, as expected for uniaxial load.

The results of X-ray diffraction on the deformed samples indicate that along with the reorientation of orthorhombic crystals there is also evidence of the stress-induced martensitic transformation of orthorhombic polyethylene to its monoclinic form. The presence of this transformation was detected at permanent plastic strains greater than 0.20. However, the amount of material which participates in this transformation is limited; at all stages of the deformation the majority of the crystals remained in their principal orthorhombic form. A detailed study of the transformation to monoclinic crystals and their orientation was very difficult because of the small amount of that phase in the samples and additionally because the monoclinic crystal reflections overlap the shoulders of much more intense peaks of the orthorhombic phase.

3.5. SAXS and WAXS Studies of Strain Recovery. All previously reported results were obtained for unloaded and fully recovered samples. In order to examine the nature of the strain recovery process, X-ray scattering experiments were carried out with samples examined first under load and then in the unloaded but not fully recovered state.

Parts a and b of Figure 10 show the SAXS and WAXS two-dimensional patterns for the undeformed specimen. Parts c and d of Figure 10 show the scattering patterns recorded for a sample deformed to a total true strain of $\epsilon = 0.24$ directly in the camera and still held under load. For this test two separate samples of identical dimensions and deformed under identical conditions to the same final strain were used in order to study the related SAXS and WAXS responses. The samples were unloaded and the SAXS and WAXS patterns were recorded both 1 h (transient strain, $\epsilon_t = 0.09$; Figure 10e,f) and 24 h (permanent strain, $\epsilon_p = 0.06$; Figure 10g,h) after unloading. Because the samples are not at equilibrium during strain recovery, the exposure times were shortened to less than 1 min. In a similar way the results for samples deformed to a total strain of $\epsilon = 0.36$ ($\epsilon_t = 0.17$ and $\epsilon_p = 0.13$) and $\epsilon = 1.22$ ($\epsilon_t = 0.77$ and $\epsilon_p = 0.71$) were obtained. The features of the scattering patterns given by the samples deformed to $\epsilon = 0.36$ were practically the same as for the samples with $\epsilon = 0.24$ and are not shown here. The patterns obtained for the samples with $\epsilon = 1.22$ are somewhat different and are shown in Figure 11. Additionally, in Table II the numerical data evaluated from the scattering patterns for all samples are presented. Examination of

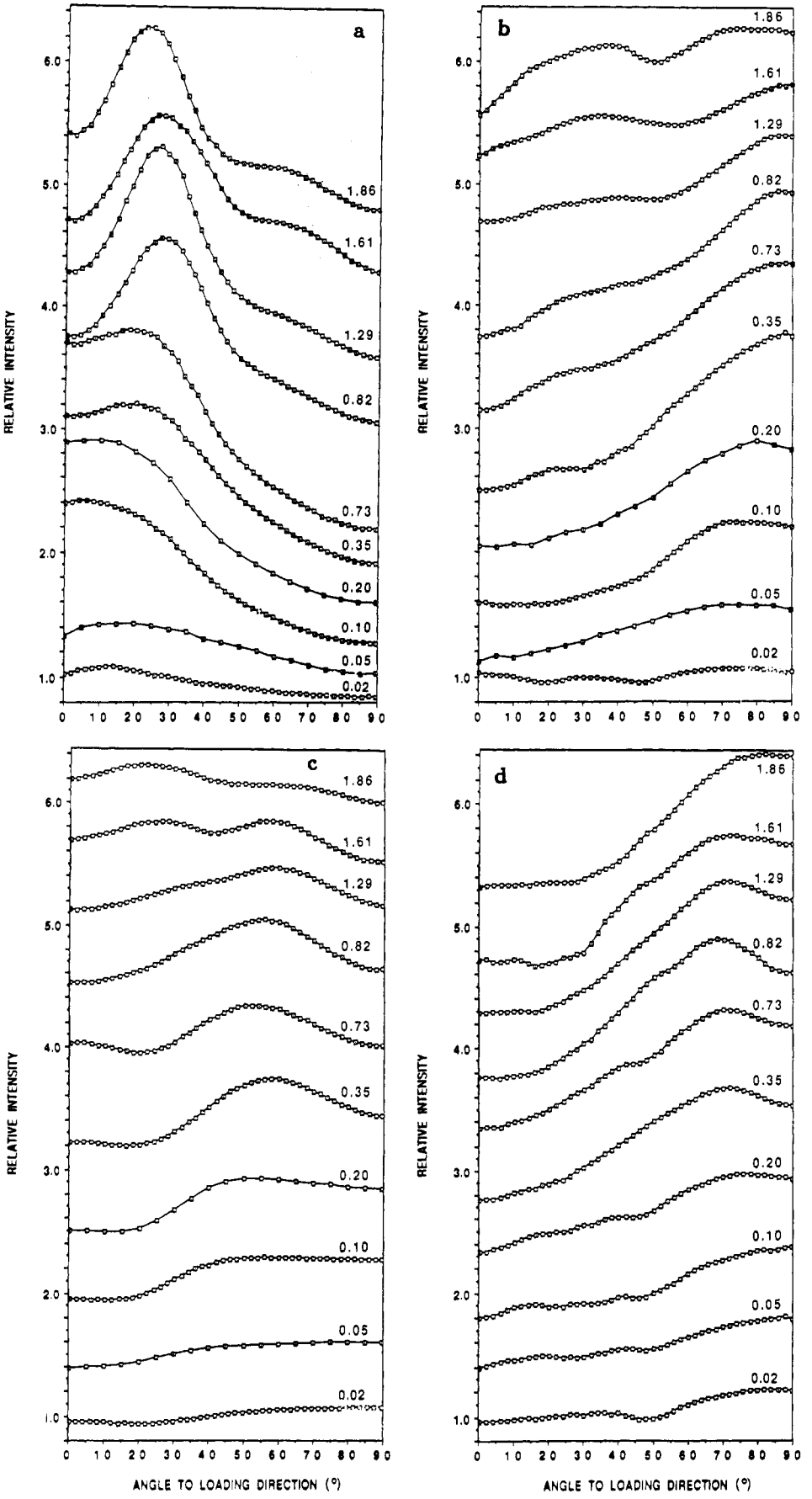

Figure 9. Plots of the dependences of the relative WAXS intensities of the diffraction by particular crystallographical planes on the altitude angle between the plane normal and the loading direction: (a) (200) plane, (b) (020) plane, (c) (110) plane, (d) (011) plane. The curves were shifted along the intensity axis for clarity.

the results presented in Figures 10 and 11 and Table I indicates that the changes in the lamellar orientation induced by deformation are reversible to some extent. Samples with the smaller levels of initial strain regained a lamellar orientation very close to that of the initial, undeformed state with nearly full strain recovery. Even for the sample deformed to $\epsilon = 1.22$, which exhibited a two-point SAXS pattern under load, a considerably more

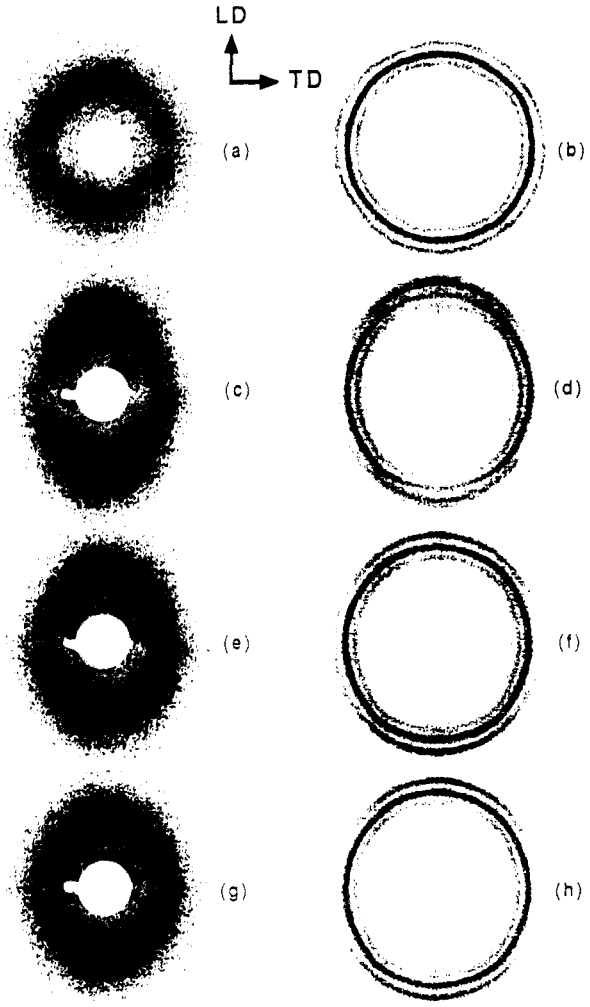

Figure 10. SAXS (a, c, e, and g) and WAXS diffraction patterns (b, d, f, and h) of compressed samples: in the initial state (a and b); deformed to a true strain of 0.24 and held under load (c and d); 1 h after unloading (e and f); 24 h after unloading (g and h).

isotropic lamellar orientation is seen after strain recovery, although of course the permanent lamellar orientation is much more intense than in less deformed samples.

The changes of lamellar orientation during a deformation–strain recovery cycle are accompanied by significant changes in crystal orientation, as indicated by the WAXS results. For smaller deformations (ϵ = 0.24 and 0.36) the normals to the (200) planes, i.e., *a* axes of crystallites, orient themselves close to the loading direction but with quite a broad distribution; normals to (110) planes orient preferably at some angle away from LD. During the strain recovery process normals to both (200) and (110) planes rotate toward LD. Note the rotation of the orientation maximum of (110) toward LD and a narrowing of the (200) arc around LD, which are both indicated in Table II. This means that the crystals rotate during strain recovery around any [*hk*0] axis toward LD, whereas at the same time the lamella normals, being more or less parallel to the [001] direction, rotate away from LD. It is important to note that such behavior indicates clearly that the recoverable part of deformation involves interlamellar sliding as the predominant deformation mechanism. During compression, the chain axis, *c*, and the lamella normal, *n*, rotate toward LD, and during the strain recovery both rotate in the opposite direction.[14] Thus, the permanent deformation remaining after strain recovery and the related crystal lattice rotations are the result of plastic deformation of the crystalline phase; there is no indication of reversibility of that crystallographic deformation in our experimental data.

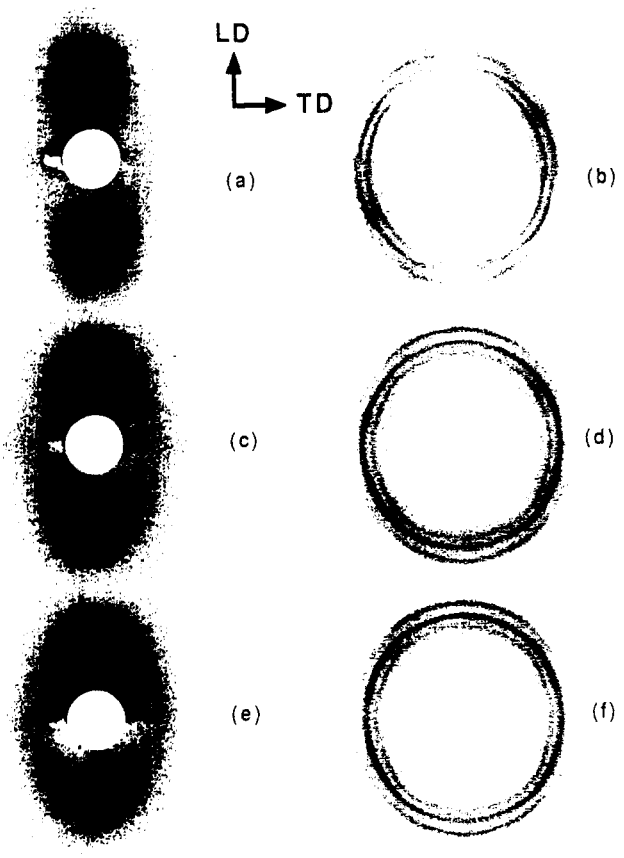

Figure 11. SAXS (a, c, and e) and WAXS diffraction patterns (b, d, and f) of compressed samples deformed to a true strain of 1.22 and held under load (a and b); 1 h after unloading (c and d); 24 h after unloading (e and f).

Similar behavior was observed for other samples deformed to higher strain (ϵ = 1.22, ϵ_p = 0.71) with the exception that the amount of plastic deformation was larger and the manifestation of the back-sliding of the lamellae during recovery was much less noticeable in the scattering patterns compared to the samples deformed to lower strains. Note the back rotation of the (110) reflections by only 3° and the practically stable position of the (200) reflection, which has now split into two arcs, each located at ca. 24° from LD. Such behavior indicates the "locking" of the interlamellar sliding process at some stage of deformation, making this deformation less reversible. The strain at which such change occurs may be estimated on the basis of macroscopic strain recovery data, supported by density measurements (Figures 2 and 3), at $\epsilon \approx 0.5$ (corresponding $\epsilon_p \approx 0.2$). Above that strain the amount of recovered strain no longer increases but remains at a rather constant level or shows, at the highest applied strains, a tendency to decrease. Such changes indicate the saturation of one of the many possible recovery paths, and our results suggest strongly that this may be related directly to the reverse interlamellar sliding mechanism discussed above.

4. Discussion

The results presented in the previous section allow us to identify the active deformation mechanisms in uniaxial compression of HDPE. The experimental results show that plastic deformation affects the amorphous and the crystalline component of the semicrystalline polyethylene and that deformation in both of these components is activated nearly simultaneously at early stages of the deformation, and both contribute to the development of

Table II
SAXS and WAXS Data for Specimens under Load and during Strain Recovery

		sample A			sample B			sample C		
	before deformation	loaded	1 h	24 h	loaded	1 h	24 h	loaded	1 h	24 h
strain	0.0	0.24	0.09	0.06	0.36	0.17	0.13	1.22	0.77	0.71
long period along LD (Å)	317	254	291	296	244	269	283	232	269	276
long period along RD (Å)	317	339	332	326	347	336	326	(0)	384	384
rel intens of SAXS at max along LD	1.0	1.10	1.04	1.01	1.28	1.17	1.14	2.07	1.86	1.45
rel intens of SAXS at max along RD	1.0	0.76	0.93	0.98	0.72	0.90	0.97	(0)	0.76	0.76
altitude angle (deg) between (110) max and LD		49	46	42	50	46	43	61	59	59
altitude angle (deg) between (200) max and LD	~0	~0	~0	~0	~0	~0	24	24	24	
altitude angular width of (200) arc (deg)	360	115	110	107	115	110	105			

the orientation of the crystalline material within the sample, as compatibility of deformation among these components demands. The basic difference between the two components is that plastic deformation of the amorphous material is partially reversible, whereas no evidence was found for reversibility of deformation of the crystalline component. Substantial strain recovery in deformed polyethylene was reported in the past by several authors.[15,16]

The mode of deformation of amorphous layers depends on their orientation with respect to the loading direction; those layers oriented perpendicular to LD undergo compression, while those parallel to LD are stretched perpendicular to that direction, and the layers in all other orientations are sheared. In all of these modes the amorphous material, which under the deformation conditions reported here is well above its glass transition, behaves as a lightly cross-linked rubber, able to undergo a substantial amount of strain recovery. The exact topological nature of the amorphous layers, and thus the strain response, is, of course, very sensitive to the molecular constitution of the material (molecular weight, polydispersity, branching) and to the history (temperature, stress, strain) of the sample-forming process.

The shear of the amorphous layers induces interlamellar sliding, that is highly reversible at low strains but becomes rather permanent above $\epsilon \approx 0.5$ ($\epsilon_p \approx 0.2$). Strain recovery of interlamellar shear was found previously in deformation of oriented polyethylene.[14,16] Such shear, in contrast to other deformation modes of amorphous material, induces additionally the reorientation of the crystalline lamellae and in this way is affecting the slip mechanisms active in the crystalline parts of the sample.

The deformation of the crystalline phase, which results in permanent orientation of the crystals, begins around the yield point and occurs simultaneously with the deformation of the amorphous material. Figure 9 shows that at a permanent strain as low as 0.02, which is slightly above the yield point, there is already a noticeable preferred orientation of the crystallographic planes. This crystallographic orientation is enhanced and undergoes some evolution as the strain increases and new mechanisms are activated. Three stages of the deformation process under uniaxial compression can be distinguished on the basis of the evolution of the (200) plane orientation (Figure 9a) in the following ranges of true plastic strain, ϵ_p: 0.02–0.20, 0.35–0.73, and 0.82–1.86. In each of these stages, the maximum of the orientation distribution of normals to (200) planes moves monotonically toward the LD with increasing strain; between these three regimes of deformation, however, there are back-rotations (i.e., away from LD) of the poles of the (200) plane.

In the first stage of deformation the pole figures of the individual crystal planes show very weak and broad maxima, especially at the lowest strain examined (i.e., 0.02–0.05; see Figure 9). The maximum in the orientation of the *a* axis (poles of 200) planes) is located near LD and shifts from ≈15° to ≈10° toward LD as strain increases from 0.02 to 0.20. At the same time the *b* axis orientation (poles of the (020) planes) starts initially from a position of 70° away from LD and moves to ≈80° from LD (Figure 9b). Normals to the (110) planes form an especially broad distribution, with a maximum in the range of 40–60° (Figure 9c). The (011) poles tend to orient themselves nearly perpendicular to LD, at 80–85°. The location of the maximum in orientation of the chain axis, *c*, can be estimated as also occurring near 80–85° from LD. Such a chain orientation is probably the result of the activity of two crystallographic slip systems acting in the (100) plane: the (100)[001] chain slip system, slip along the (100) plane in the direction of the chain axis, [001], and the (100)[010] transverse slip (which is slip in the same plane but in a direction parallel to [010] and, therefore, perpendicular to the chain axis). These two slip systems in polyethylene are known to have the lowest plastic resistances. The critical resolved shear stresses required to activate these systems are 7.2 and 12.2 MPa, respectively,[17] whereas other deformation mechanisms need shear stress higher than 14–15 MPa to be activated.[1,3,17,18] The (100)[001] chain slip system causes rotation of the *a* axes of the crystallites toward LD and *c* away from it, both rotations occurring around the *b* axis, whose orientation remains unaffected by this deformation mechanism. The (100)[010] transverse slip induces the rotation of *a* toward LD and *b* away from it, both around *c*. Thus, the simultaneous activity of both slip systems would induce the change of orientation of *a* toward LD and at the same time *b* and *c* away from this direction, which we have indeed observed experimentally. The (100)[001] chain slip system is expected to dominate over the (100)[010] transverse slip because of its lower plastic resistance. It is unclear whether these slip processes act simultaneously in the common (100) planes of the same crystallites or they act in two different populations of crystals, each oriented preferentially for a particular slip to occur. Here we note that at the initial phases of deformation, when the texture is poorly developed, the locations of the orientation maxima for particular planes are not necessarily correlated; the maximum of orientation of the (200) plane normals may come from the diffraction on crystallites oriented differently from those contributing to the maximum of the (020) orientation.

The striking feature of the orientation distributions is that the various maxima develop very close to the loading and radial directions. Starting with an unoriented sample, the active slip systems would be expected to lead to orientation maxima somewhere near 45° from LD, because crystals oriented with slip planes at 45° from LD have the highest resolved shear stress, so the slip should be initiated first in crystals in this orientation range. The deformation process is still in its initial stage so that large rotations of crystals are not likely to occur. Nevertheless, the max-

imum of the orientation of the a axis is experimentally observed to move rapidly very close to LD. This suggests that in addition to the crystallographic slip processes considered some other mechanism must be active too. The evidence indicates that this mechanism was the reversible lamellar shear, discussed above. That mechanism acting in the amorphous layers probably starts before the onset of the crystallographic slip processes as might be expected from their near rubbery behavior, inducing the rotation of both the a and b axes of crystals away from LD. These reoriented lamellar crystals are then deformed plastically by (100)[001] and (100)[010] slip processes, which cause the rotation of a toward LD and b and c away from it. Upon unloading the sample, the interlamellar shear reverses, which in turn causes the rotation of a and b of the deformed crystals back toward LD. As a result the maximum of orientation to the a axis is closer to LD than expected if only the crystallographic slip systems were active. This is clearly observed experimentally in specimens with low strains ($\epsilon_p < 0.20$).

There is not much evidence in our data of the activity of other deformation mechanisms at low strains, especially slip systems in (010) and (110) planes, which should induce rotations of poles of these planes toward LD. At the strain $\epsilon_p = 0.02$ the small maximum of the b axis orientation near LD can be distinguished, but it disappears for higher strains. This may suggest some limited activity of the (010)[001] slip system in the initial deformation stages. This mechanism must have been limited only to the crystals with the most favorable orientation producing the highest resolved shear stress for this particular slip system. There is no evidence of the (110)[001] slip system activity. However, near permanent strains of 0.20 twinning on (110) and (1$\bar{1}$0) planes may become active, albeit its evidence is very vague.

At strains between 0.20 and 0.35 an unexpected (based on the active crystallographic slips) change of orientation of the a axis occurs. In spite of the activity of the (100) slip system, which always induces rotation of a toward LD, the maximum of the a axis orientation moves away from LD; for $\epsilon_p = 0.35$ it is located near 20°, whereas it was at 10° for $\epsilon_p = 0.20$. The maximum of b axis orientation shifts from 80° ($\epsilon_p = 0.20$) to about 86–88° ($\epsilon_p = 0.35$). Maxima of orientation of normals to (110) and (011) planes develop near 58° and 72°, respectively. The estimated position of maximum orientation of the c axis would shift accordingly from ≈80° ($\epsilon_p = 0.20$) to ≈71° ($\epsilon_p = 0.35$). To understand this change in orientation of the a axis at strains above $\epsilon_p = 0.20$, we should recall that it is in this strain range that the "locking" of interlamellar shear occurs; therefore, at this strain and above deformation is much less reversible on unloading. Because of this locking there is almost no shift of the a axis orientation toward LD on unloading, as was the case for smaller strains, and the position of the orientation maximum in the unloaded state remains similar to that under load. For the same reason the maximum of the b axis orientation moves closer to the radial direction, perpendicular to LD. The orientation maxima, especially for (110) and (011) poles, are better developed for a strain of 0.35 than for 0.20 because of a more advanced crystallographic orientation and the ceasing of the reverse shear of the interlamellar material on unloading which does not disturb any further the orientation produced by crystallographic slip. At smaller strains the lamellae rotated back around any [hk0] axis, resulting in broadening of the orientation distribution in recovered samples.

The shapes of the orientation distribution curves for $\epsilon_p \geq 0.35$ are additionally modified by the stress-induced martensitic transformation of orthorhombic crystals to the monoclinic modification, which apparently starts in this strain range (see the previous section). Annealing at 120 °C of the sample with $\epsilon_p = 0.35$ led to the disappearance of the monoclinic phase and the flattening of the orientation maximum of the a axis between 0° and 20° (the shape of the curve for the annealed sample resembled more closely the shape observed for $\epsilon_p = 0.20$) which indicates that during deformation some of the crystallites oriented with their axes almost parallel to LD transformed to the monoclinic form. The martensitic transformations of such oriented orthorhombic crystals of polyethylene were previously observed by Seto et al.[19] and by Young and Bowden.[18] The influence of the martensitic transformation on the evolution of the texture is, however, quite slight, since the amount of monoclinic phase produced was relatively small. On the other hand, Seto et al.[19] showed that monoclinic crystals that formed under load are metastable and largely transform back to the orthorhombic form on unloading of the sample. Thus, we can not exclude the possibility that the amount of the monoclinic phase in our specimens under load might actually have been higher than observed after unloading and strain recovery; hence, the martensitic transformation may have contributed more toward the evolution of the texture during the deformation process.

A third deformation process, albeit of marginal importance, sets in the strain range of $\epsilon_p = 0.35$–0.73. This is the twinning process upon unloading, which is probably of the {310} type. The indication of this mechanism is the small maximum appearing in the orientation distribution of the b axis at about 20° from LD (Figure 9b). That maximum develops better for higher strains and its formation is most likely the result of {310} twinning of the crystals with their axes oriented close to 18.5° from LD and the b axes close to 71.5° and c axes perpendicular to LD. For crystals with this particular orientation the resolved shear stress for {310} twinning, resulting from tensile stress along LD, is highest. Therefore, the crystals oriented in that way are predisposed to undergo unloading twinning since such unloading can be considered as the superposition of a tensile increment of deformation. As a result of this postulated {310} twinning a maximum should appear for a at 71.5° and for b at 18.5° via rotation of poles by 53° around the c axis. Experimental data in the range $\epsilon_p = 0.35$–0.73 indicate only the presence of a small orientation maximum of near 20° from LD, but it appears strongly at larger strains, simultaneously shifting away from LD as a result of activity on the (100)[010] slip system. The maximum in the a orientation expected at the 71.5° position is absent or too small to be detected, but it is clearly seen near 70° at higher strains. Because the maximum in orientation of the b axis is not present after annealing, its presence could be a result of unloading relaxation twinning.[20] Because the orientation changes related to the postulated twinning are very small, we cannot exclude the possibility that these observed changes are related to twinning of the {110} type on crystals with a slightly different orientation (a parallel to LD, b and c perpendicular to LD) followed by (100) slips in the twinned crystals. The postulated {310} twinning, similar to the martensitic transformation, increases its activity with increasing strain, as may be seen in Figure 9a,b. Nevertheless, both mechanisms play only a minor role compared to (100) crystallographic slip systems which dominate the deformation process. Figure 9a demonstrates that with the increase of strain to $\epsilon_p = 0.73$ the axis orientation maximum moves toward LD, which proves continuing

activity on these slip systems.

At $\epsilon_p = 0.82$ there is a noticeable change in the distribution of the *a* axis orientation. At that strain the maximum of the orientation curve moves again back, away from LD, and there is a further relative decrease in the population of the crystallites with the *a* axis parallel to LD, making this maximum at about 30° more distinct. Such orientation changes may be connected with the kinking of some of the lamellae and the formation of deformation bands which, as indicated by morphological observations with light and electron microscopy, are known to begin in this range of strain (Figures 4 and 5). Lamellar kinking produces a remarkable change of orientation of a considerable fraction of crystals still oriented with *a* nearly perpendicular to LD, transforming them suddenly to orientations in which *a* now resides at an acute angle with respect to the radial direction. This probably causes the shift of the *a* axis orientation maximum away from LD. Because the orientation of the *b* axis at this stage of deformation does not change too much compared to lower strains, it seems that kinking of lamellae involves slipping and breaking of the crystals along (*h*00) planes.

After initiation of the kinking-induced reorientation processes at strain near $\epsilon_p = 0.8$, the orientation maximum of the *a* axis begins once again to move toward LD with increasing strain, indicating that crystallographic slip systems on the (100) planes are still active. Additionally, at $\epsilon_p = 1.29$ a new minor maximum in the *a* orientation develops near 70°, which was expected for twinning on unloading. The maximum in orientation of *b* observed previously at ca. 20° and connected with twinning becomes stronger and shifts toward larger angles (away from LD), suggesting increased activity of the twinning process as well as slip systems in the (100) planes. In contrast to the maximum reported for $\epsilon_p \geq 0.35$, the maxima in *a* and *b* orientations which are present now do not disappear during annealing; the neighborhood of twinned crystals is relatively free of residual stresses, and, therefore, these crystals are stable in the twinned form. This is possible if twinning occurred not on unloading but earlier, during loading of the specimen, a process which could happen if the crystals fragmented during lamellar kinking. That phenomenon probably generated the appropriate local stress to induce twinning of neighboring crystals already oriented with their *a* axes near LD. As discussed earlier the {310} twinning of such oriented crystals should induce formation of a new maximum in the orientation distribution of the *a* axis near 71.5°, a maximum in orientation of *b* near 18.5° and an increase of orientation of the poles of the (110) planes near 15.5° and 52.5°. Simultaneously, in the latter distribution, the density of poles oriented near 37.5° and 74.5° should decrease. The orientation curves determined experimentally show such features, although the respective maxima are located mostly at angles slightly higher than expected.

It is somewhat surprising that the twinning mode active at large strains is {310} and not {110}, which was probably active at low strains. Both of these twinning modes are activated by similar levels of shear stress and produce the same amount of shear strain.[1-3] In most of the experimental studies of polyethylene deformation the {110} twinning mode was found as the dominant, although it was also reported that in heavily deformed polyethylene {310} twinning may be a substantial mechanism as well.[21,22] Preedy and Wheeler[22] showed that in tensile deformation {110} twinning occurs at relatively low strains and that the {310} twinning mode becomes active under the condition of large strain during which the crystal morphology is changed from lamellar to microfibrillar. That behavior is similar to what we have observed; {310} twins are generated at high strains during the lamellar kinking process, producing some destruction and rearrangement of the crystallites. The state of the internal local stresses at this moment is unclear but evidently favors in some way the {310} twinning mode. Further deformation of twinned crystals by slip probably makes these crystals stable and the deformation not reversible on annealing. The slip that can become active in the twinned crystals is mostly (100)-[010], as suggested by the shift of the orientation maxima for the *b* axis toward larger angles (initially 20° to 32° for $\epsilon_p = 1.86$).

The final texture of the deformed material ($\epsilon_p = 1.86$) is axisymmetric, with a well-developed orientation of the *a* axis nearly parallel to LD. Most poles of (200) planes are tilted with respect to LD by ca. 22°. The preferred orientation of the *b* axis is close to the radial direction, but the orientation distribution is broader than for the *a* axis and disturbed additionally due to twinning. The positions of major maxima in the orientation distribution of the poles of (020) and (110) planes suggest that the molecular axis, *c*, is tilted about 10° away from the radial flow direction, i.e., almost perpendicular to LD. The orientation curve for the poles of (110) (and ($1\bar{1}0$)) planes exhibits two low and flat maxima at positions matching the postulated texture. Most probably because of the increasing activity of the twinning process with increasing strain, the maximum located closer to LD develops somewhat more at the expense of the other one located closer to the radial direction. Such features of orientation, if probed with less sensitive methods, may give the impression of rotation of the (110) poles toward LD and hence be interpreted as being the result of (110)[001] chain slip. While such an interpretation cannot be completely rejected, we think that the main source of the observed changes in the (110) and ($1\bar{1}0$) plane orientations is the above-mentioned twinning process.

Finally, after discussion of this detail in the development of the fiber morphology upon uniaxial compression we must point out the fundamental difference that it has when compared with the morphology that develops in extensional deformation of fiber drawing, rolling, and plane strain compression in all of which a clear and strong orientation alignment of molecules occurs. In all of these latter extensional deformations the initial set of amorphous layers are first rendered inactive by being rotated "out of the way" to have their plane normals (the normals to the crystal/amorphous boundaries) *n* become nearly perpendicular to the *c* axis of the chains. This, however, is followed by a more or less disruptive fragmentation of strongly elongated lamellae that reconstitutes the old amorphous material into a new long period nearly perpendicular to the chain axis. Thus, in the eventual texture the amorphous plane normals, *n*, and the molecular axes, *c*, become nearly parallel. In uniaxial compression where molecule axes are aligned nearly parallel to the radial flow direction the extended lamellae apparently do not undergo fragmentation in the same wholesale manner and the amorphous material layers remain rotated "out of the way" with their plane normals, *n*, remaining parallel to LD and thus perpendicular to the chain axis, *c*. This should give a fundamentally different set of elastic properties to the uniaxially compressed disks such as unusually high and isotropic elastic stiffness in the plane of the disk and rather moderate to low stiffness in the thickness direction of the disks. Such properties have not been reported in the past and are worthy of study in their own right.

5. Conclusions

1. The results of morphological and structural studies of semicrystalline HDPE deformed under uniaxial compression demonstrated that the plastic deformation process is made up of a continued series of transformations from the initial to the final oriented state.

2. Although deformation was carried out to true strains close to 2, comparable to those encountered in cold drawing, rolling, or plane strain compression, no major discontinuities in transformation similar to micronecking, or lamellar fragmentation, found in the latter modes of deformation were observed. The morphology of uniaxially compressed polyethylene remained lamellar over the whole range of strains studied, and the discontinuous transformation of lamellar crystals into microfibrils did not occur. The results reported here show clearly that such discontinuous transformations are not necessary in the deformation of semicrystalline polymers to attain high strains.

3. The deformation of HDPE by uniaxial compression, although continuous, is a complex, multistep process. At various deformation stages some additional mechanisms are activated to allow further deformation. Both amorphous and crystalline regions of the polymer contribute importantly to the deformation process. The role of the amorphous phase is especially important because polymer crystals generally lack five independent slip systems necessary for compatible deformation of polycrystalline assemblies. While the amorphous material does not remove this restriction entirely, it materially aids the deformation.

4. In the slowly crystallized linear polyethylene used here we found that the deformation of the amorphous phase was recoverable to a very significant degree upon sample unloading. The strain recovery saturated at a total applied strain of $\epsilon = 0.5$.

5. The deformation of the amorphous material does not directly influence the orientation relations within the crystalline phase, but it is able to modify the orientation of the stacks of lamellar crystals by interlamellar shear. In this way the deformation of the amorphous material plays a significant role in the development of the overall texture of the deformed polymer.

6. The deformation of the amorphous phase is followed by plastic deformation of lamellar crystals. According to our findings, deformation in the crystals involves mechanisms which are entirely crystallographic in nature that are well-known from the previous extensional deformation studied. Among these mechanisms the two crystallographic slip processes of (100)[001] chain slip and (100)-[010] transverse slip play the leading part in the deformation over the whole range of strain studied. These two slip systems are known to have the lowest plastic resistances in polyethylene crystals. Other slip systems with higher resistances were not detected. The deformation by these slip processes operating in the (100) plane was supported by (010)[001] chain slip and two twinning modes, {110} and {310}, activated at various stages of deformation but limited to crystals with specific orientations with respect to the direction of the load.

7. At moderate strains the deformation of the specimens tended to localize into a dense set of very fine shear bands, inside of which the crystallographic slip processes must have been active. Because of the fine scale of these bands, the overall deformation is quasi-homogeneous. The deformation bands were initiated by kinking of those lamellae which had been oriented along the loading direction. The formation of the kinks is the only discontinuous transformation during the whole deformation process, and it is limited to the small fraction of suitably oriented crystallites.

8. In summary, inside the lamellar crystals the main active mechanisms contributing most to their deformation were the (100)[001] and (100)[010] crystallographic slip processes acting together with the mechanisms of shear deformation of the amorphous phase, giving substantial interlamellar sliding.

Acknowledgment. This research was supported by a DARPA–URI program administered by ONR under Contract No. N00014-86-K-0768.

References and Notes

(1) Bowden, P. B.; Young, R. J. *J. Mater. Sci.* **1974**, *9*, 2034.
(2) Haudin, J. M. In *Plastic Deformation of Amorphous and Semicrystalline Materials. Ed. Phys.* **1982**, 291.
(3) Lin, L.; Argon A. S., to be published.
(4) Peterlin, A. *J. Mater. Sci.* **1971**, *6*, 490.
(5) Peterlin, A.; Corneliussen, R. *J. Polym. Sci., Polym. Phys. Ed.* **1968**, *6*, 1273.
(6) Peterlin, A.; Balta-Calleja, F. J. *Colloid Polym. Sci.* **1970**, *242*, 1093.
(7) Keller, A. *J. Polym. Sci.* **1955**, *15*, 31.
(8) Galeski, A.; Bartczak, Z.; Argon, A. S.; Cohen, R. E. *Macromolecules*, in press.
(9) Krause, S. J.; Hosford, W. F. *J. Polym. Sci., Polym. Phys.* **1989**, *27*, 1853.
(10) Ahzi, S.; Argon, A. S.; Bartczak, Z.; Lee, B. J.; Parks, D. M., to be published.
(11) Kanig, G. *Kolloid Z. Z. Polym.* **1973**, 782.
(12) Adams, W. W.; Briber, R. M.; Sherman, E. S.; Porter, R. S.; Thomas, E. L. *Polymer* **1985**, *26*, 17.
(13) Song, H. H.; Cohen, R. E.; Argon, A. S. *Macromolecules* **1990**, *23*, 870.
(14) Young, R. J.; Bowden, P. B.; Ritchie, J. M.; Rider, J. G. *J. Mater. Sci.* **1973**, *8*, 23.
(15) Sargent, C. M.; Shinozaki, D. M. *Scr. Met.* **1977**, *11*, 401.
(16) Pope, D. P.; Keller, A. *J. Polym. Sci., Polym. Phys.* **1975**, *13*, 533.
(17) Bartczak, Z.; Argon, A. S.; Cohen, R. E. *Macromolecules*, in press.
(18) Young, R. J.; Bowden, P. B. *Philos. Magn.* **1974**, *29*, 1061.
(19) Seto, T.; Hara, T.; Tanaka, K. *Jpn. J. Appl. Phys.* **1968**, *7*, 31.
(20) Hay, I. L.; Keller, A. *J. Polym. Sci.* **1966**, *1*, 41.
(21) Levis, D. L.; Wheeler, E. J.; Maddams, W. F.; Preedy, J. E. *J. Polym. Sci.* **1972**, *10*, 369.
(22) Preedy, J. E.; Wheeler, E. J. *J. Mater. Sci.* **1977**, *12*, 810.

Registry No. Polyethylene, 9002-88-4.